CHAPTER 2 REVIEW AND THEORY

This chapter remarks the introduction to diamond-like carbon (DLC), structure and properties of DLC, the related theories, documents, and research topics which are related to DLC film deposition by filtered cathodic vacuum arc method, and characterization of DLC films. The effect of thermal heating on DLC of previous studies will also be reviewed.

2.1 Introduction of magnetic recording head and fabrication process

The schematic of hard disk drive (HDD) and magnetic recording head is shown in Figure 2.1. The key components of HDD are magnetic recording disk for data storage and magnetic recording (MR) head for read and write data. The detail of MR head is shown in Figure 2.2.

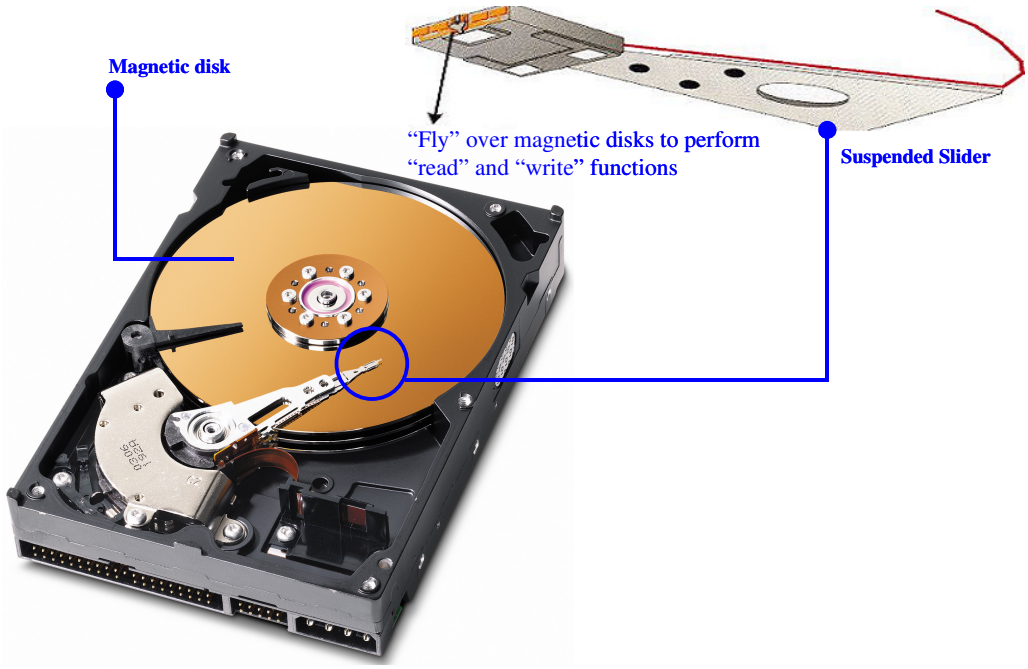

Figure 2.1 The schematic of hard disk drive

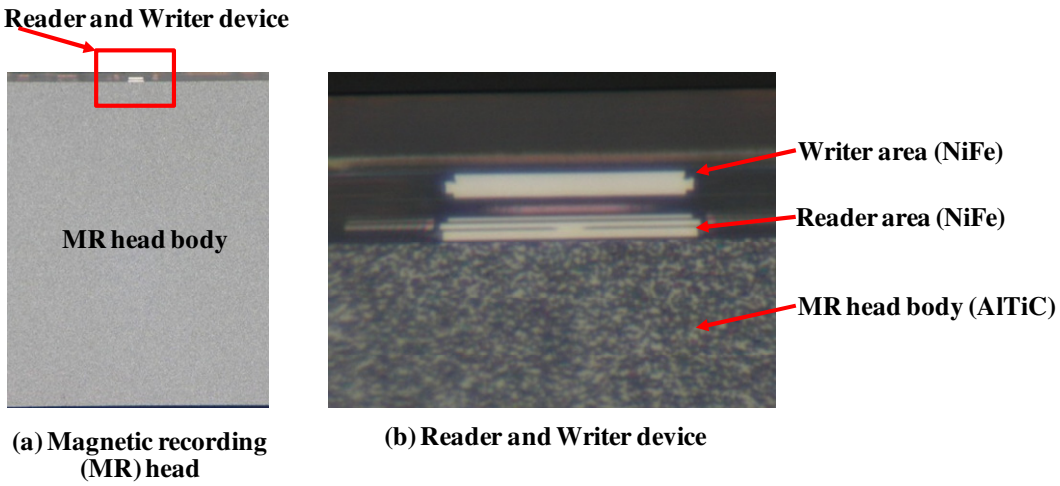

Figure 2.2 (a) Magnetic recording head; (b) Reader and Writer device.

The fabrication of magnetic recording heads is briefly described. Key processes of magnetic recording head fabrication are listed as follows;

Machining: wafer was sliced to 6" bar form and bar was divided to be 2" bar form for next process

Lapping: lapping process was performed to get open reader and writer device. Magnetic resistance is the key parameter to measure and let us know the end of lapping process.

DLC Coating: DLC (Diamond-like Carbon) film was coated on magnetic recording head for corrosion protection

Patterning (Photolithography and Etching): to perform read and write function, magnetic head has to fly over magnetic disk by aerodynamic force. The patterning on magnetic head has been designed to lift off and maintain the flying height between head and disk during perform the read/write function

Quasi-Static test: electrical test to specify the good and bad part in term of reader performance

Head Dicing: another process of machining to divide the bar to be individual slider form

Inspection: to separate the mechanical fail head

Figure 2.3 shows key processes of magnetic recording head fabrication.

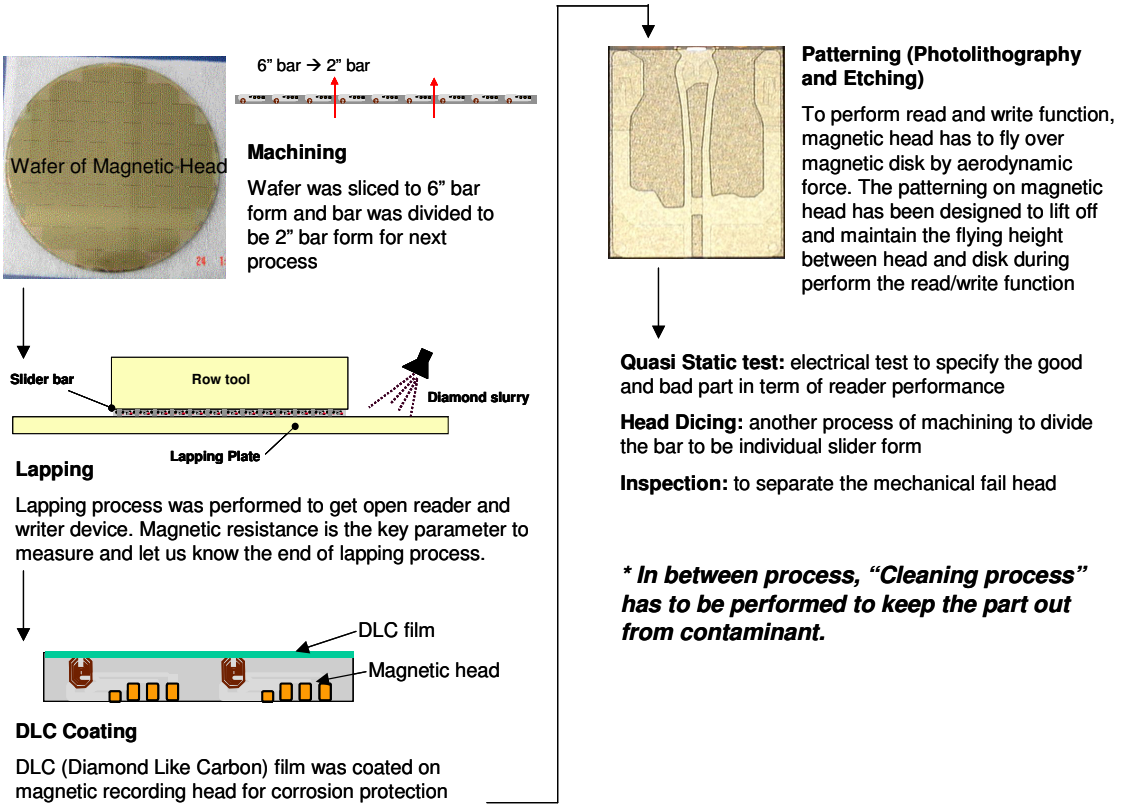

Figure 2.3 Key processes of magnetic recording head fabrication.

2.2 Introduction of Diamond-like carbon (DLC) [14]

Diamond-like carbon (DLC) is a metastable form of amorphous carbon consisting of a mixture of sp^3 and sp^2 carbon structures, where sp^2-bonded graphite-like clusters are embedded in an amorphous sp^3-bonded carbon matrix. They can be roughly divided in hydrogenated and hydrogen-free DLCs. In the case where hydrogen atoms are present in the random network as bound to C, they stabilize the sp^3 hybridization, which is responsible for high hardness and rigidity of the network, and they decrease the connectivity between the sp3 hybridized C sites, which influences the film mechanical properties. DLC materials have many potential applications due to their superior themal, electronic, optical, mechanical and tribological properties. It has been used as protective coatings in areas such as optical windows, magnetic storage, car parts, biomedical coatings and as micro-electromechanical devices (MEMs). The properties of DLC material are closely related to their bonding structure, which is in turn determined by the deposition conditions.

2.3 Structure of Diamond-like carbon [14]

Carbon forms a great variety of crystalline and disordered structures because it is able to exist in three hybridizations, sp^3, sp^2 and sp^1 (Figure 2.4). The electronic configuration of a carbon atom (C) is $1s^2 2s^2 p^2$ and therefore it has 4 electrons in its outer shell. Electronic bonds can be classified in σ and π bonds according to their symmetry. Hybridized orbitals can form by the combination of the wave functions of s and p orbitals. The possible hybridizations of the C atom are described in Table 2.1.

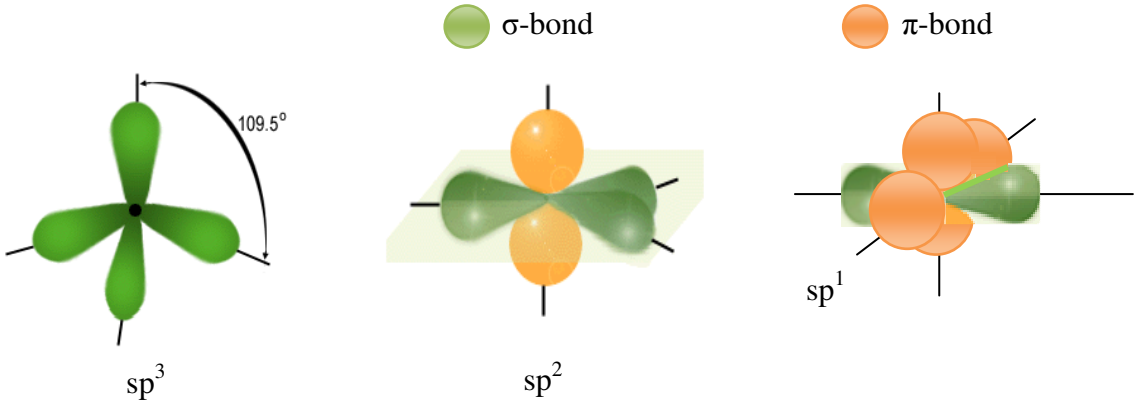

Figure 2.4 sp^3, sp^2 and sp^1 configuration

Table 2.1 The hybridization of carbon atom

Hybridization	Contributing orbitals	Angle between hybridized orbitals	Typically found in
sp^1	$s+p_x = 2\ sp^1$	180	Organic molecules
sp^2	$s+p_x+p_y = 3\ sp^2$	120	Graphite, Organic molecules
sp^3	$s+p_x+p_y+p_z = 4\ sp^3$	109.5	Diamond, Organic molecules

In the four-fold coordinated sp^3 configuration as in diamond, a carbon atom's four valence electrons are each assigned to a tetrahedrally directed sp^3 orbital, which makes a strong σ bond to an adjacent atom. In the three-fold coordinated sp^2 configuration as in graphite, three of four valence electrons enter trigonally directed sp^2 orbitals, which form σ bond in plane. The fourth electron of the sp^2 atom lies in a p-π orbital, which lies normal to the σ bonding plane. The π orbital forms a weaker π bond with an π orbital on one or more neighboring atoms. In the sp^1 configuration, two of the four valence electrons enter σ orbitals, each forming an σ bond directed along the $\pm$ *x*-axis, and the other two electrons enter p-π orbital in the *y* and *z* directions.

The ternary phase diagram, first used by Jacob and Moller, displays the compositions of the various form of amorphous C-H, as in Figure 2.5. The lower left hand corner show disordered graphite ordering, such as glassy carbon, evaporated a-C. The right hand side shows hydrocarbon polymer and limitation in a triangle that C-C cannot forms.

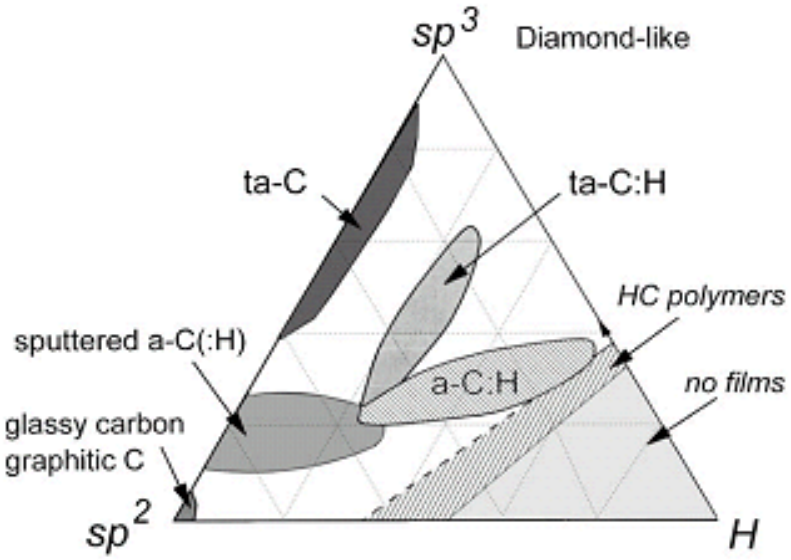

Figure 2.5 Ternary diagram, sp^2, sp^3, and H-Content of ta-C, ta-C: H, a-C:H, and a-C

Various deposition methods has been developed to produce amorphous carbon to achieve high sp^3 bonding. Mckenzie suggested to call this high sp^3 fraction as tetrahedral amorphous carbon (ta-C), to distinguish it from sp^2 a-C. Typical properties of the various forms of DLC are compared to diamond and graphite in table 2.2.

Table 2.2 Comparison of major properties of amorphous carbons with those reference materials diamond, graphite, C60 and polyethylene

Type of carbon	Sp^3 (%)	H (%)	Density (g/cm^3)	Gap (eV)	Hardness (GPa)
Diamond	100	0	3.515	55	100
Graphite	0	0	2.267	0	
C60	0	0		1.6	
Glassy C	0	0	1.3-1.5	0.01	3
Evaporated C	0	0	1.9	0.4-0.7	3
Sputtered C	5	0	2.2	0.5	
ta-C	80-88	0	3.1	2.5	80
a-C:H hard	40	30-40	1.6-2.2	1.1-1.7	10-20
a-C:H soft	60	40-50	1.2-1.6	1.7-4	<10
ta-C:H	70	30	2.4	2.0-2.5	50
Polyethylene	100	67	0.92	6	0.01

2.4 Deposition process [14]

The key property of DLC is its sp^3 bonding. The deposition process which promotes sp3 bonding is a physical process, ion bombardment. The highest sp^3 fractions are formed by C^+ ions which ion energy around 100 eV.

The mechanism of the formation of sp^3-hybridized C is modeled as “subplantation”, where energetic C atoms are able to penetrate the material and subsequently bond in a

highly stressed tetrahedral (sp^3) configuration. To penetrate the growing DLC network, the ions must overcome the C displacement energy, between 25 and 35 eV. This energy is considerably higher than the typical energy of evaporation deposition (0.3 eV) or sputtering (3-5 eV), but can be achieved via energetic deposition techniques such as pulsed laser deposition (PLD, atom energy up to 40 eV) or filtered cathodic vacuum arc (FCVA), in which the major portion of the upcoming C atoms is ionized, and a bias can be applied to the substrate to accelerate the C ions up to the desired energy. In the latter case, it has been determined that the final sp^3 fraction can be as high as 90 % when the C ions energy is about 100 eV. When the majority of the upcoming ions are not ionized, as is the case of magnetron sputtering, it can be inferred that a certain degree of film bombardment by Ar ions, also accelerated by an applied substrate bias, would provoke the formation of sp^3 C. The individual C atoms on top of the growing film would be knocked-down as a consequence of the energy transfer between incident Ar ions and C atoms. Indeed, it has been reported that large fractions of sp^3 C are also obtainable via magnetron sputtering/ion plating (MS/IP).

The fraction of sp^3 bonding of DLC is a key interest property. In addition, sp^3 bonding is normally form by ion bombardment or physical process.

The review of this topic is summary from J.Robertson. The terms of low energy surface implantation introduced as “subplantation” by Lifshitz et al., with explain that the sp^3 was produced by preferential displacement of sp^2.

The nuclear stopping occurs when incident ions got elastic collision with target. Ions will lose their energy with a few monolayer of range. The energy of ion, which can penetrate surface layer of substrate, is called the penetration threshold (E_p). The minimum energy required for ion to displace a bonded atom to create vacancy interstitial pair is the displacement threshold (E_d). The surface binding energy (E_B) is energy of surface of solid. The net penetration threshold for free ion is

$$E_p \sim E_d - E_B \tag{2.1}$$

The surface binding energy E_B is equal to 7.4eV for carbon. With displacement’s energy of graphite is 25eV then $E_p \sim$ 32eV. Hence, an incident ion with lower energy than *Ep* will not able to penetrate substrate, so it will remain in the lowest energy state as sp^2 on the surface. If the energy of incident ion is higher than *Ep*, The local density will be increased since it has probability that ion can penetrate surface and enter a subsurface interstitial site. The local density made reforming of new local bonding around. In case of high energy such as incident ion, ion bombardment on existing film creates a changing of atomic hybridization, become more sp^2 for a low density and sp^3 for high-density species. The ranges depend on ion energy, increase energy made a penetration is deeper and the heat dissipation to displacement atoms is 30% when ions penetrate into a surface. The whole process involves three step start with collision by incident ions about 10^{-13} s, then a thermalization about 10^{-12} s and the final stage is a relaxation after 10^{-10} s.

The schematic of subplantation process is shown in Figure 2.6. The penetration can be found in two way, direct or indirect (knock-on, occurs for case of ion assisted deposition)

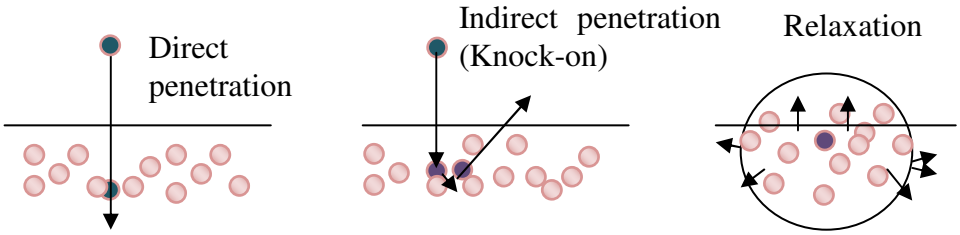

Figure 2.6 Schematic of basic subplantation process

2.5 Filtered cathodic arc deposition overview

2.5.1 Filtered cathodic arc deposition

DLC deposition process using cathodic arc plasma consists of highly ionization of carbon charge ion from graphite cathode. Filter cathodic arcs, thin films deposition techniques with energetic ions species. The plasma generate by arc discharge of cathode material. The plasma parameters including ion charge state of +1, mobility about $2x10^4$ m/s with corresponding ion energy 25eV. The comparison of DLC overcoat for magnetic recording head between FCA deposition with ECR-CVD and IBD has been review by N. Akita et al. [15] their system schematic is from Shimadzu Corp., as shown in Figure 2.7.

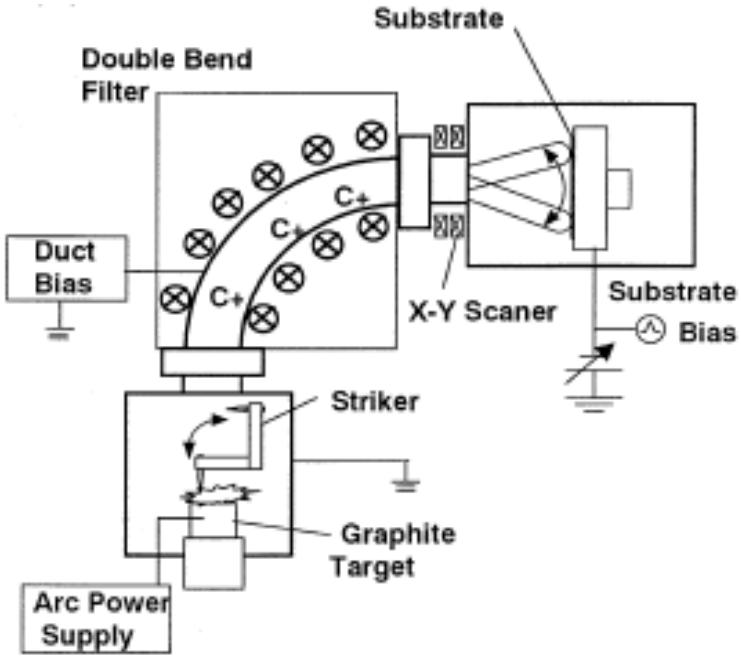

Figure 2.7 Schematic of filter cathodic arc system

FCA system usually consists of graphite as a cathode material connects with high current arc power supply. The igniter is used to ignite plasma or cathode spot that are two techniques such as contacting with striker, and or high voltage between anode and cathode.

The filter is magnetic generated by coil using to homogenized plasma and filter out macro particle from arcing. The second path of external magnetic field is used for uniformity adjustment. Definition of arcs have been introduced by Andres [33] as a high current of electrical discharge (greater than 1A) and low voltage (lower than 50V), they are characterized by a collective electron emission mechanism from cathode that divided into thermionic and explosive (or cathodic arc)). Thermionic required high temperature cathode and often assisted by electric field to reduce minimum energy required for electron emission. With high temperature, allow energetic electrons are able to overcome a potential barrier. In contrast, cathodic arcs are able to operate with a cathode near room temperature. Electron emission occurs at hot, non-stationary, micron size of cathode spots, extremely high current density, power density and plasma density.

Anders [16] proposed that operation of cathode arcs spot has a rapid sequence of microexplosions. The cathode martial has phase transformation at the area of spot appeared, resulting in fully ionized and rapidly expanding plasma. Material molecules between dense plasma from arcs discharge and much colder cathode were changed in liquid phase, ejected by plasma pressure, as droplet called “macroparticles,” often found under shallow angle of cathode surface. In contrast to arc discharge, glow discharge often has low current and high voltage, electron emission from cathode by individual process that contributes by primary excited electron or photon.

Comparison report from previous experiments show G-peak appear near 1580 cm^{-1} and D-peak near 1350 cm^{-1}, ECR-CVD and IBD show H percent in higher wave number because the use of hydrocarbon gas and a-C:H formation while DLC film from FCA produced ta-C (tetrahedral amorphous carbon) from a purely C^{+} and zero H content. However, there are similar results between three difference types of growth in optical properties at 632.8nm.

2.5.2 Particle filter system and plasma transport efficiency

A magnetic filter is one of important component for filter cathodic arc deposition system. The magnetic filter is used to separate and remove particles from the cathodic arc plasma, or homogenized plasma.

The filter configuration often construct with coil to generate magnetic field. The review of various type of particle filter was introduced by Anders [16]. He proposed that the efficiency of particle filter was defined as ration between ion current and arc current. The ion current can be measured by a Langmuir probe with constant negatively bias, in addition the arc current detected at power supply. The system constant k or alternative name called plasma transport efficiency is used to characterized arc filter system as

$$k = \frac{I_{ion}}{I_{arc}} \tag{2.2}$$

The filter system was develop to improve plasma transport efficiency while minimize particles. The major concept for filter to eliminate or separate particle from plasma are the trajectory of particle is in straight line while the motion of electrons are in spiral along magnetic field, and ions will be guide due to they are charge particles.

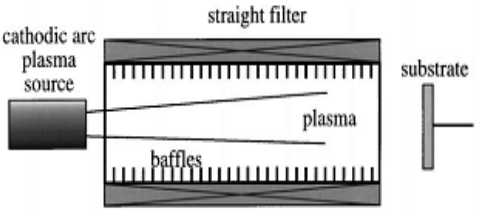

(a) Straight magnetic filter

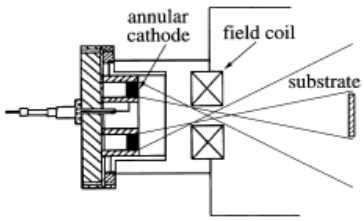

(b) Straight magnetic filter combined with cathode plasma source

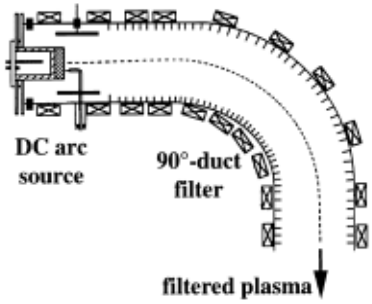

(c) Classic 90 degree duct filter

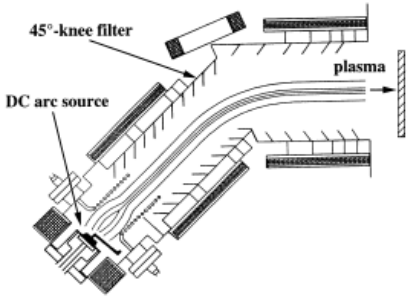

(d) Knee-filter

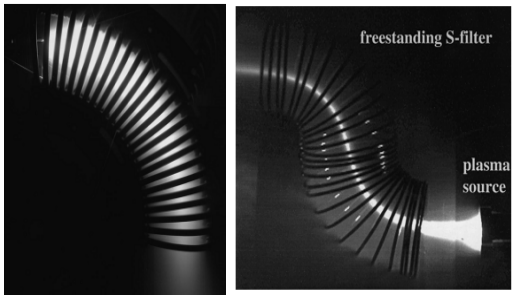

(e) Freestanding 90 degree filter and Freestanding S-filter

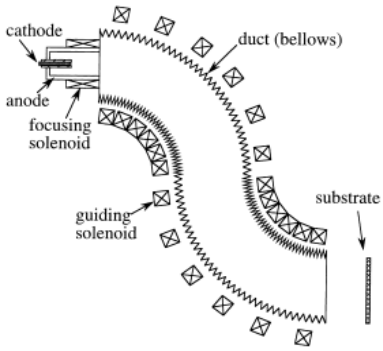

(f) S-duct filter

Figure 2.8 Sample of magnetic filter system

The simple filter is straight magnetic filter which located in straight line, as show in Figure 2.8 (a) this filter improve plasma to particle ration but there is a line of sight that made this system could not efficient to eliminate particle at the substrate. The propose of using straight magnetic filter combine with annular cathode plasma source is to eliminate a line of sight, system shown in Figure 2.8 (b).

Some filter develop in angle or curve such as classic 90 degree duct filter, as Figure 2.8 (c). Plasma stream can bend through the angle or curve but particles motion is a straight trajectory then collected by duct. The advantage of this system is low plasma transport efficiency. However, it can be improved by duct bias. The Knee-filter as Figure 2.8

Figure (d) was design to reduce plasma loss from the classic 90 degree duct filter by reduce angle to 45 degree and angle of duct use 45 degree

The freestanding 90-degree filter is alternative from classic 90-degree duct, as show in Figure 2.8 (e) this filter is no duct, magnetic field generate by few turns coil with high current. Particle may stick on the coil or leave through opening between coils. The freestanding S, Figure 2.8 (e) or S-duct filter, Figure 2.8 (f) are similar concept as freestanding 90 degree, or classic 90 degree duct filter however the S curve is purpose to offset shift from the first curve.

2.6 Characterization of DLC films

The availability of reliable characterization tools for carbon films down to a few atomic layer thicknesses is one of the most decisive factors for technology development and production. In particular, non-destructive techniques are preferred.

2.6.1 Raman spectroscopy for microstructure characterization [14, 17-20]

Raman spectroscopy is based on the phenomenon discovered by Raman and Krishran that, when monochromatic light passed through matter, a very small fraction of the scattered light consists of light whose wavelength is longer than the original incident light. Raman spectroscopy is one of the analytical techniques which can and has been used to study carbon films. This technique has a combination of features which make it particularly attractive for evaluating the carbon as following:

(1) It is non-destructive.
(2) It can be carried out in the atmosphere.
(3) It can have a spatial resolution of the order of microns.
(4) No physical contact is necessary.
(5) It is particularly sensitive to the structure of carbon films.

The Raman spectra depend on
(1) Cluster of the sp^2 phase
(2) Bond length and bond angle disorder
(3) Presence of sp^2 rings or chains
(4) The sp^2/sp^3 ratio
These factors act as competing forces on the shape of the Raman spectra, as shown schematically in Figure 2.9.

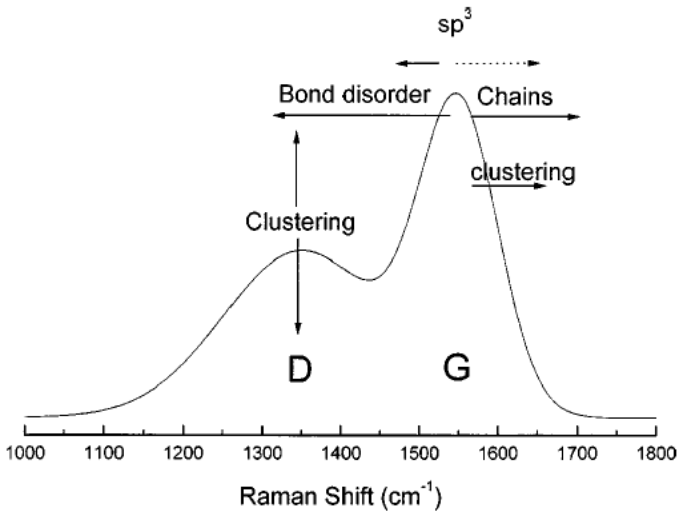

Figure 2.9 Schematic diagram of influences on the Raman spectra. A dotted arrow marks the indirect influence of the sp^3 content on increasing G position.

In visible Raman spectra the cross-section of the sp^2 phase is much higher (50-250 times for 514 nm) than the one of the sp^3 phase. Furthermore, the spectra directly depend on the quality or configuration of the sp^2 phase and only indirectly on the quantity of the sp^3 phase. Most times the sp^2 configuration varies consistently with the sp^2 fraction; however, in some cases, the sp^2 quality can be changed independently form the sp^2:sp^3 ratio. This phenomenon, which we called hysteresis, typically happens for high temperature deposition, annealing after deposition, low dose ion implantation of ta-C or unfiltered deposition process.

Diamond (sp^3) has a single Raman active mode at 1332 cm^{-1}, and single crystal graphite (sp^2) at 1580 cm^{-1}. Amorphous carbon structure has a mixture of sp^2 and sp^3. Visible excitation Raman spectroscopy use 488nm or 514nm laser. Excited photons has limitation because the sp^2 sites have a greater cross-section thus a spectrum of amorphous carbon appears due to sp^2 sites only which has two modes G and D, the G peak lie at around 1560 cm^{-1}, and the D peak around 1350 cm^{-1}. The G peak is due to bond stretching of all pairs of sp^2 atoms in both rings and chains. The D peak is due to the breathing modes of sp^2 atom in rings as shown in Figure 2.10.

UV excitation Raman spectroscopy, first study Gilkes et al. C-C sp^3 vibration can be detected as the T peak around 1060 cm^{-1}. The T peak is not appearing with visible excitation Raman spectroscopy. They explain that the Raman spectra of an amorphous solid is proportional to the total vibration density of states (VDOS) multiplied by cross-section. However, in DLC case is that excitation with photon energy 2.4eV (514 nm) dominates to the π–π^* transitions at sp^2 sites and this gives a resonant enhancement of their cross-section. Using ultraviolet (UV) excitation with photon energy 5.1eV (244nm) dominate on both sp^2 and sp^3 sites, and this provides more information of sp^3 structure in DLC film.

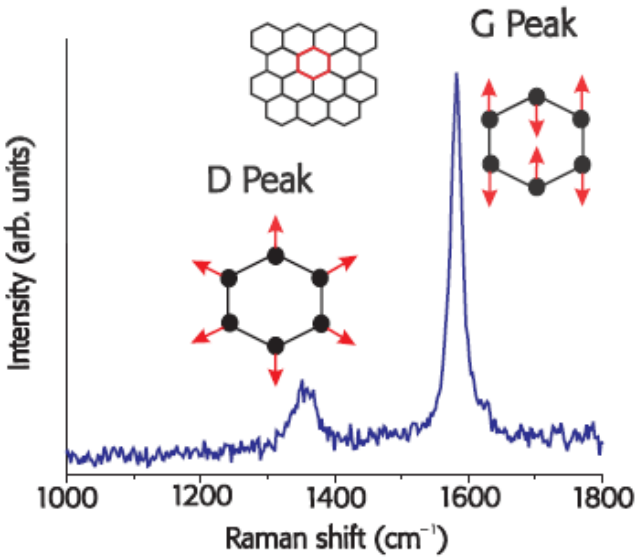

Figure 2.10 514 nm Raman spectrum of highly orientated graphite, show nuclear displacements associated with each vibration

A.C. Ferrari and J. Robertson study resonant Raman spectroscopy of disordered, amorphous, and diamond like carbon with various excitation wavelength such as 229, 244, 325, 351, 458, 514.5, 532, 633, and 785nm (5.41-1.58eV). The variation in G-peak position can be found with changing photon excitation energy and T peak found at Raman shift ~1060cm^{-1} using UV excitation (Figure 2.11).

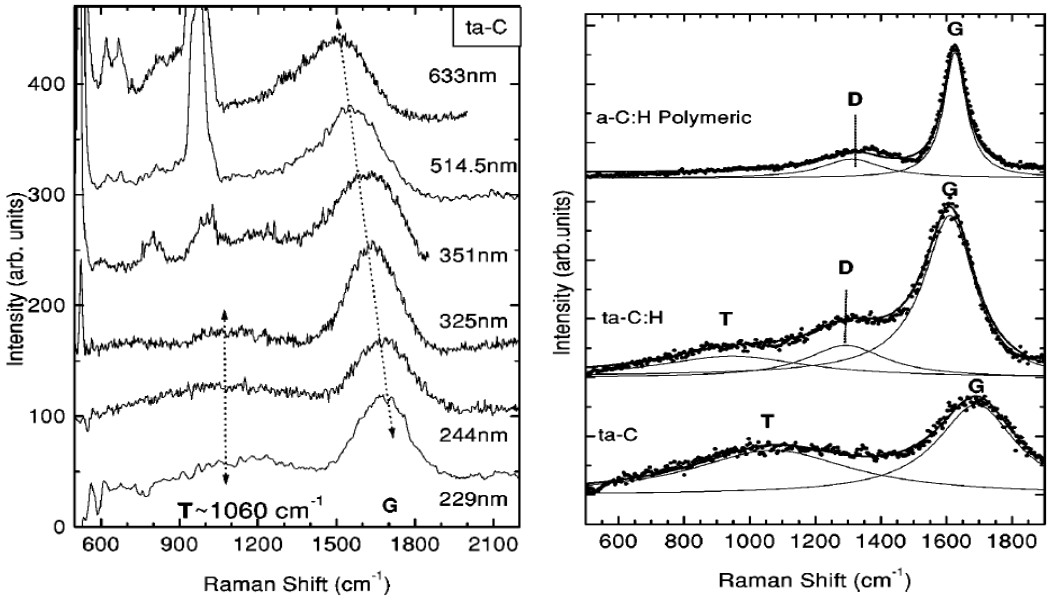

Figure 2.11 Raman Spectrum of Multi-Wavelength and UV excitation (a) Multi-Wavelength Raman Study of Ta-C (Tetrahedral Amorphous Carbon) Film; (b) Raman Spectrum of a-C:H Polymeric,Ta-C:H and ta-C using 244nm UV excitation

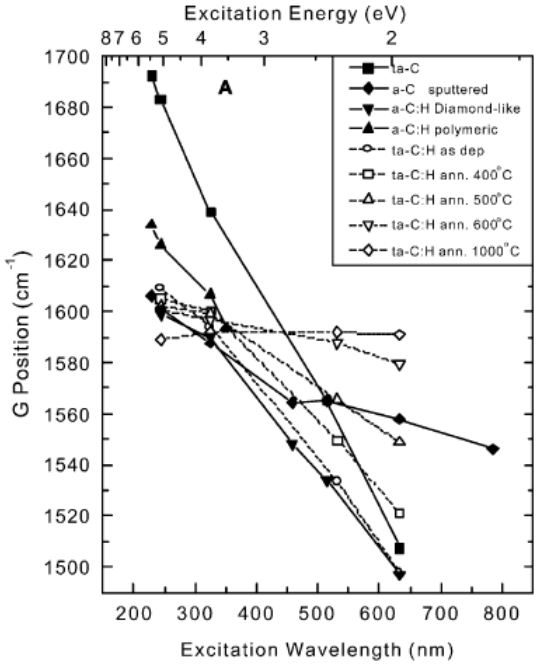

Figure 2.12 Dispersion of G peak vs. excitation wavelength, bottom x axis, and energy, top x axis, for a series of template samples.

A.C. Ferrari studied the variation of the G peak position with excitation wavelength and energy (Figure 2.12) and found that the physical behavior of the G peak in disordered graphite is radically different from amorphous carbons, even though the G peak positions might accidentally be the same at some excitation energy. The G peak in graphite cannot disperse because it is the Raman-active phonon mode of the crystal. In nc-graphite, the G peak shifts slightly upwards at fixed excitation energy due to phonon confinement, but it cannot disperse with varying excitation energy, still being a density of states feature.

2.6.2 X-ray photoelectron spectroscopy for material composition characterization [17, 20-21]

Electron spectroscopy is a technique that uses characteristic electrons emitted form a solid for elemental analysis, not for imaging as in electron microscopy. The characteristic electrons (either Auger electrons or photoelectrons) exhibit characteristic energy levels, revealing the nature of chemical elements in specimens being examined.

The X-ray photoelectron is an electron ejected from an electron shell of an atom when the atom absorbs and X-ray photon.

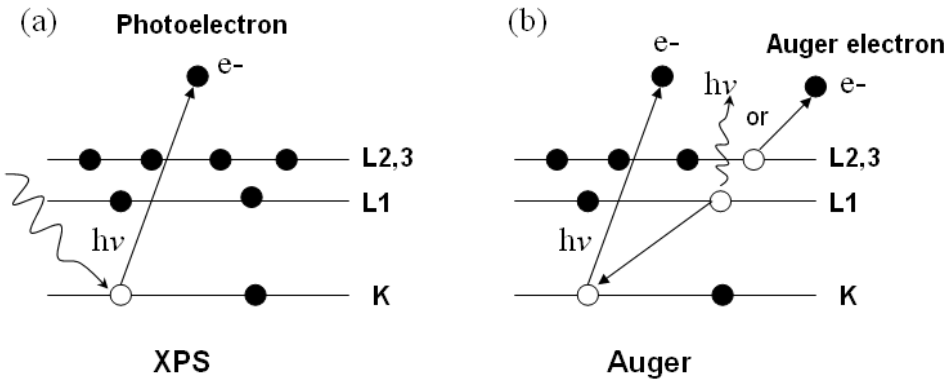

Figure 2.13 Emission processes of characteristic electrons: (a) a 1s photoelectron; and (b) $KL_1L_{2,3}$ Auger electron

Figure 2.13 schematically illustrates the emission of photoelectron from and atom when it is excited by an X-ray photon. An incident X-ray photo can have sufficient energy (a value of hν) to know out an inner shell electron, for example from the atom's K shell. In such a case, the K-shell electron would be ejected from the surface as a photoelectron with kinetic energy E_K. Knowing the kinetic energy E_K, we can calculate the binding energy of the atom's photoelectron (E_B) based on the following relation

$$E_B = h\nu - E_K - \square \qquad (2.3)$$

$\square$ is the parameter representing the energy required for an electron to escape form a material's surface, *h* is Planck's constant and v is the frequency. The value of $\square$ depends on both the sample material and the spectrometer. The binding energies (E_B) of atomic electrons have characteristic values, and these valued are used to identify elements, similar to the way the characteristic X-ray energy is use in X-ray spectroscopy. X-ray photoelectron spectroscopy (XPS) indentifies chemical elements from the binding energy spectra of X-ray photoelectrons. A typical XPS spectrum is a plot of intensity versus binding energy. Photoelectrons are ejected from different electronic shells and subshells. Each binding energy peak is marked as and element symbol plus a shell symbol from where the photoelectron was emitted.

The presence of peaks at particular energies therefore indicates the presence of a specific element in the sample under study - furthermore, the intensity of the peaks is related to the concentration of the element within the sampled region. Thus, the technique provides a quantitative analysis of the surface composition and is sometimes known by the alternative acronym, ESCA (Electron Spectroscopy for Chemical Analysis).

The most commonly employed x-ray sources are those giving rise to
(1) Mg Kα radiation (hν = 1253.6 eV)
(2) Al Kα radiation (hν = 1486.6 eV)

Peak positions in an XPS spectrum are likely to be affected by spectrometer conditions and the sample surface. Before XPS peak identification, we often need to calibrate the binding energy. Calibration is particularly important for samples with poor electrical conductivity. Calibration can be done with an internal standard that has a peak that

shows little or no chemical shift, for example, elemental Si. The most common method is use of the C1s peak at 285 eV from carbon absorbed on the sample surface.

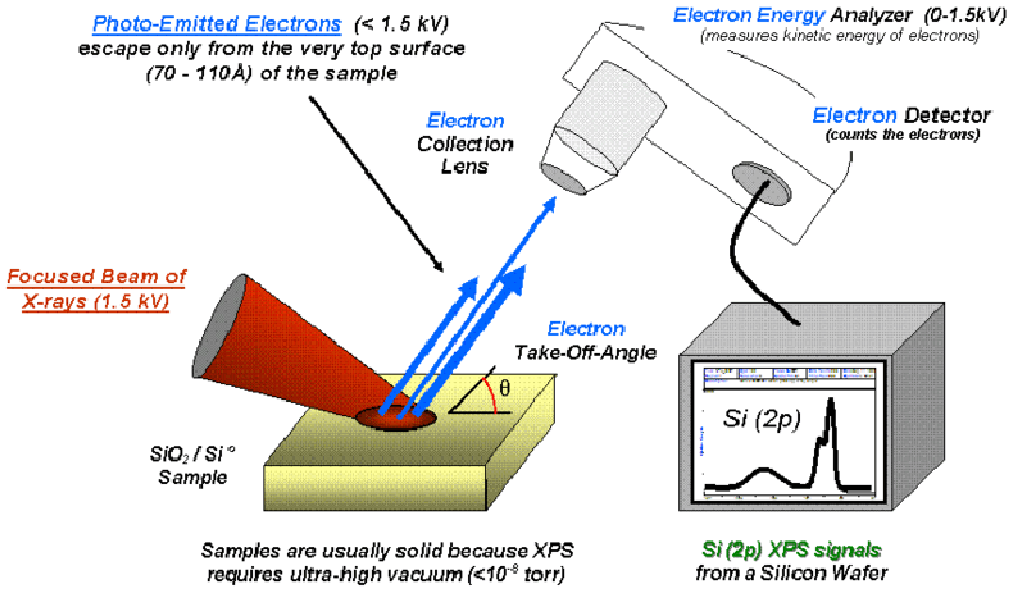

Figure 2.14 Basic components of a monochromatic XPS system

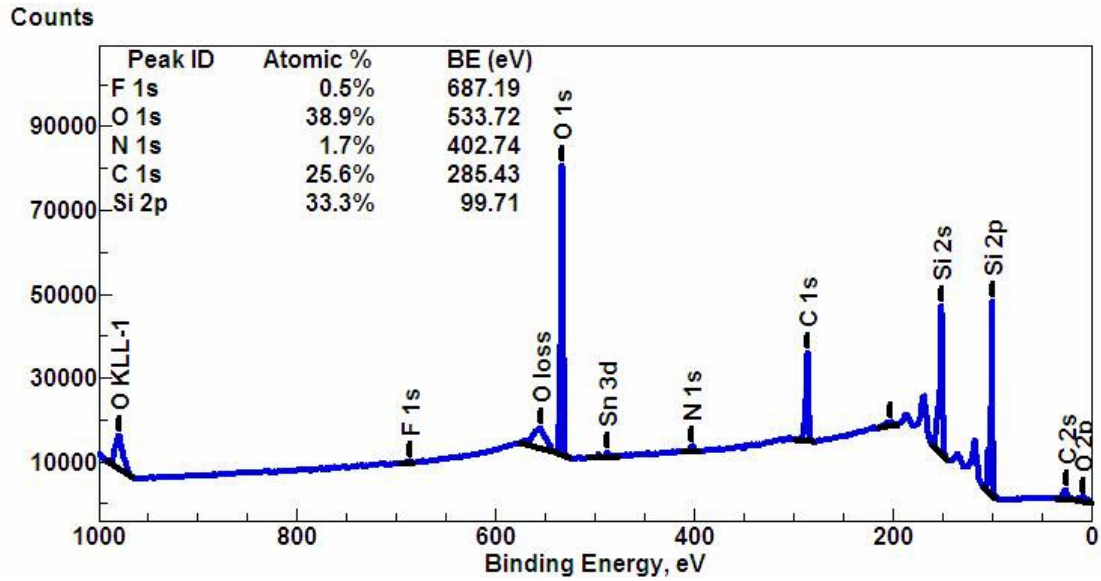

Figure 2.15 Wide-scan survey spectrum for all elements

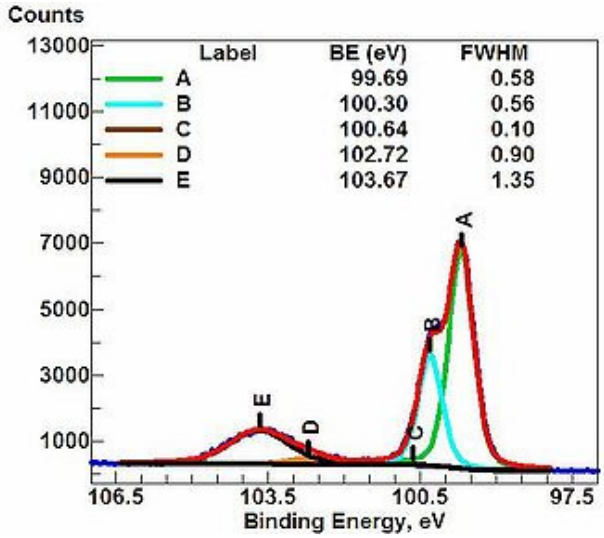

Figure 2.16 High-resolution spectrum for Si (2p) signal

XPS also can characterize the changes in composition with distance from a surface plane. The most commonly used method to obtain a depth profile of composition is sputtered depth profiling using an ion gun. The ion gun provides a flux of positively charged argon ions with current density of 1-50 uAmm^{-2} and energy of 0-5-5 keV. The ion beam bombards a sample, causing it to eject atoms from the surface. A ratering ion beam directed at a surface produces a crater. We can obtain a profile of near-surface compositions by examining the XPS spectra of the crater at its different depths.

Quantitative analysis of depth profile, in addition to quantifying concentrations, needs to measure depth accurately. There are several factors we should aware of for resolution of depth measurement.

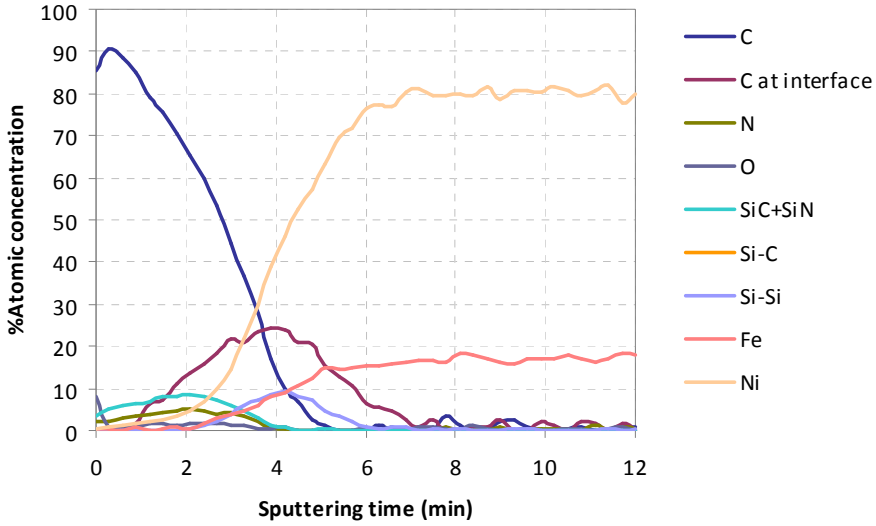

Figure 2.17 XPS depth profile of a SiN/C on NiFe coupon

2.6.3 Ellipsometry for optical property characterization [22]

Ellipsometry, also known as polarimetry or polarization spectroscopy, is a technique developed to obtain the thickness and optical constants of mono- and multi-layer dielectric films. Ellipsometry offers a nonconductive method for estimating film thickness and optical dispersion based on the interaction of polarized light with the samples. Ellipsometry, based on scientific theories from Brewster, Fresnel, Lord Rayleigh and Drude, measures and interprets the change of polarization state that occurs when a polarized beam is reflected at non-normal incident angle from a film surface. Since ellipsometry does not rely on interference effects, determination of film thickness does not depend on the wavelength of light. It is important, however, to understand the several basic concepts for ellipsometry measurement.

Electromagnetic waves consist of mutually perpendicular electric and magnetic fields, both also perpendicular to the propagation direction of monochromatic light wave. In ellipsometry measurements, only the electric field $\vec{E}$ is relevant, by considering two sinusoidal oscillating components, i.e., parallel (E_p) and perpendicular (E_s) to the plane of incidence, as shown in Figure 2.18.

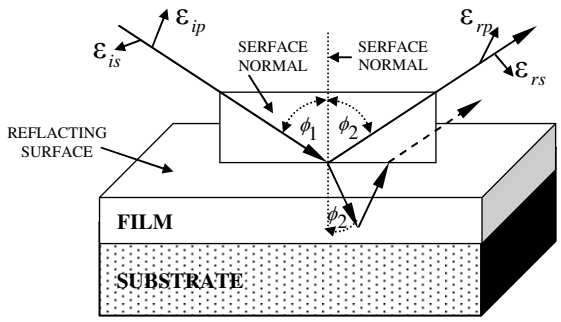

Figure 2.18 Reflection of a light beam from a surface showing refraction, reflection and polarization effects

The plane-polarizes light in the plane of incidence, consisting of the transverse oscillating electric fields, is exposed on a surface with incident, reflective, and refractive angle are ϕ_1, ϕ_2 and ϕ_3, respectively. Interaction with the surface causes both the phase and the amplitude of the reflected light components to change, relative to the incident light. The changes in form of elliptical polarization and attenuation are also shown.

Generally, the *p*-wave and *s*-wave are not necessarily in phase. Let the phase difference between the *p*- and the *s*-wave before and after the reflection be δ_1 and δ_2 respectively. The phase shift, Δ, induced by the reflection, can be defined as:

$$\Delta = \delta_1 - \delta_2 \tag{2.4}$$

In addition to a phase shift, the amplitude of the *p*-wave and the *s*-wave will also decrease due to the reflection. The total reflection coefficient for the *p*-wave and the *s*-wave is defined as the ratio of the outgoing wave amplitude to the incoming amplitude, in which they give:

$$\tan\Psi = \frac{|R_p|}{|R_s|} \tag{2.5}$$

where $|R_p|$ and $|R_s|$ are the magnitudes of decreasing amplitudes, and tanΨ is a real number. However, the two components of reflectivity R_p and R_s are generally distinct. Therefore, a complex reflection coefficient is defined, yielding the fundamental equation of ellipsometry:

$$\rho = \frac{R_p}{R_s} = \frac{E_{rp}/E_{ip}}{E_{rs}/E_{is}} = \tan\Psi e^{i\Delta} \tag{2.6}$$

The magnitude of ρ is contained in the tanΨ part and the phase of ρ is contained in the exponential function. The quantities Δ and Ψ must be measured by ellipsometer. While Δ is the phase difference that develops between the *s*- and *p*-wave components after reflection, the quantity tan Ψ is related to the amplitude ratio, and hence in ρ. These properties can be extracted out of probing light beam, making the point that the quantities which ellipsometer measures are Δ and Ψ, which are always correct. When a thin film is present on the substrate, Δ and Ψ now also depend on λ, ϕ_1, complex refractive indices (*n* and *k*) and the film thickness. Quantities such as thickness and optical constants are calculated and deduced based on assumed model, generally requiring computer analysis.

2.6.4 Nanoindentation for wear resistance characterization [23]

Nanoindentation is widely used to characterize mechanical properties of thin films. The indenter with load will applied on the surface of substrate, as show in

Fig 2.19. Load and displacement data will be capture for analysis.

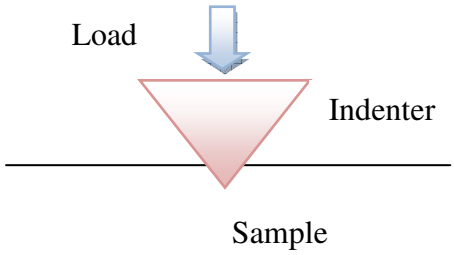

Figure 2.19 Simple schematic of nanoindenter

Nanoindentation is the ideal method for testing DLC films due to its subnanometer depth sensitivity and low load and displacement control. The ability to test the mechanical properties of such thin films without measuring the underlying substrate is what makes nanoindentation the most accurate method for mechanical property analysis.

The resulting films varied in thickness up to100 nm depending on the method used. Cube Corner diamond probe was used to calculate the mechanical properties of the films. Wear tests were made with 4 passes in a 6x6 μm track at varying force.

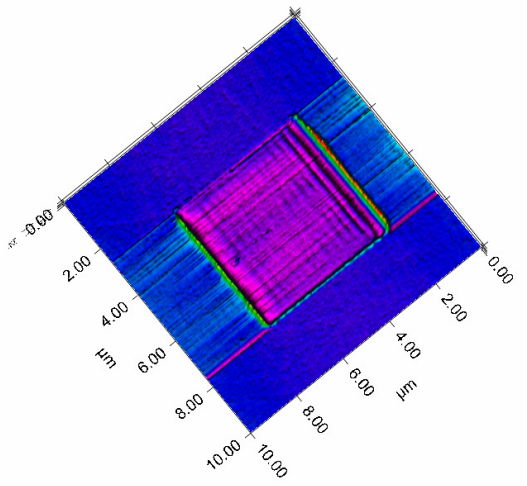

Figure 2.20 SPM image of wear track made on DLC film to determine wear resistance of coating.

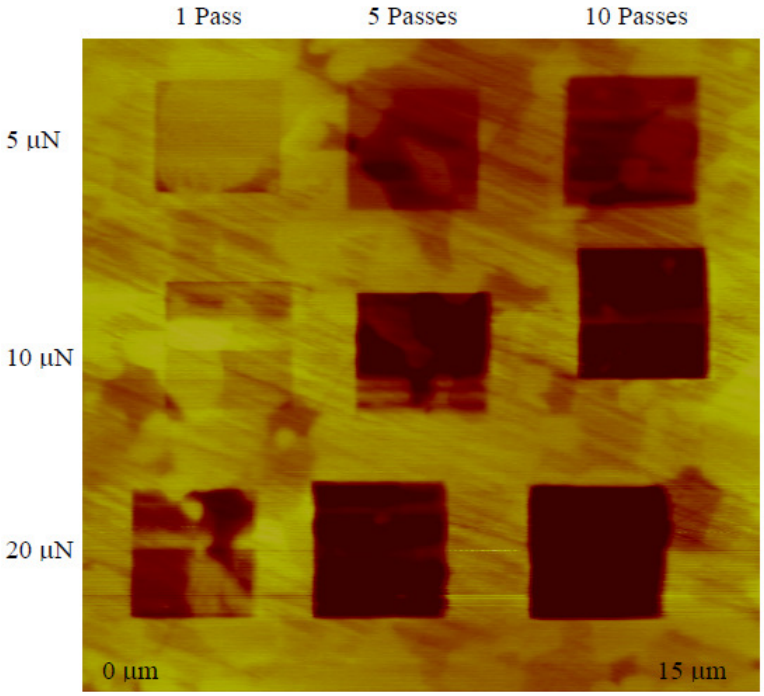

Figure 2.21 ScanningWear test on DLC (Diamond like Carbon) coating on a computer hard disk drive with 5 µm, 10 µm and 20 µm loads and 1, 5 and 10 passes respectively

Wear test is wearing resistance evaluation under abrasive wear condition and the latter a wear resistance evaluation under fatigue condition. The ta-DLC films have high abrasive wear and fatigue resistance, properbly because of their high hardness and excellent adhesion between film and substrate [32].

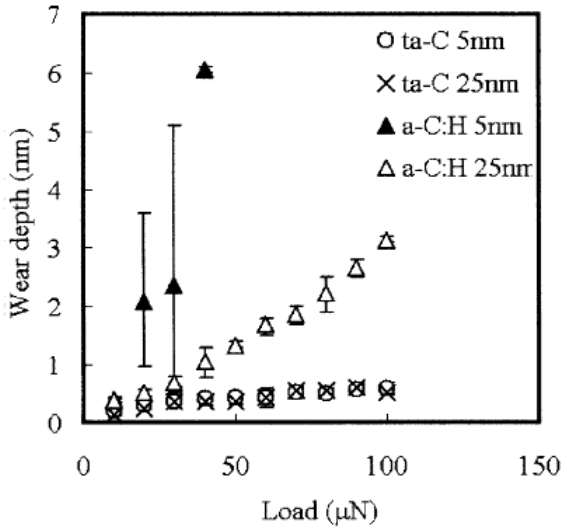

Figure 2.22 Variation of scanning-scratched wear depth of ta-C and a-C:H films with applied load [24]

2.6.5 Corrosion resistance test on magnetic recording head

For magnetic recording applications, a major concern of the cathodic arc process is macroparticle formation at the cathode during carbon evaporation. By using a macroparticle filter, macroparticles can be reduced significantly. From SEM and AFM analysis, the size of macroparticles is typically in the range of sub-micrometers in diameter. If the particles pass through the filter and land on the substrate surface during film deposition, these macroparticles will create pinholes since the over-coat thickness is less than 10 nm. An acid etch method was developed to evaluate ta-C film macroparticle contamination and pinhole density.

In the study of H. Han et al. [25], the 5-nm ta-C films were deposited on Si wafers which were pre-coated with 20 nm NiFe (Fe 18%) by DC ion beam sputtering. The coated samples were immersed in a nitric acid solution (0.1 M in water) for 10 min. After DI water rinse, the samples were analyzed by optical microscope to count pinhole density. Table 2.3 gives the acid etch test results and the comparison to 7 nm RF ion beam CVD DLC films. The pinhole density is converted into pinholes/pico-slider for clarity and the pinhole density for 5 nm ta-C is 50% less than that of the ion beam CVD process.

Table 2.3 Summary of acid etch corrosion test

Sample	Pinhole density (#/cm^2)	Pinholes/pico-slider
DLC (7 nm)	450	0.5
ta-C (5nm)	230	0.2

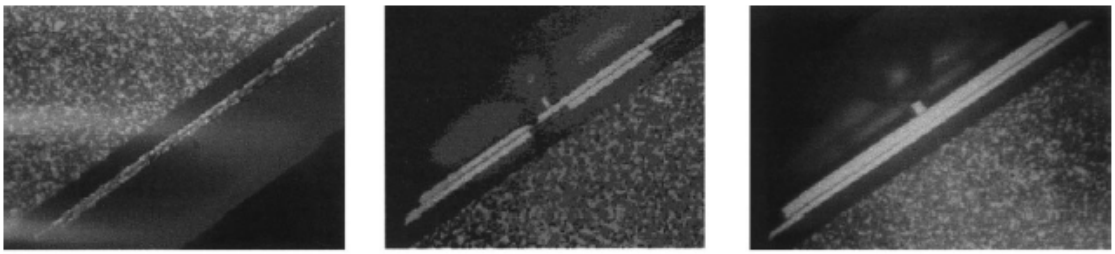

Figure 2.23 Acid etch corrosion test results for sliders with: (a) no overcoat; (b) ion beam CVD DLC, 5 nm; and (c) FCA coated ta-C, 5 nm.

2.6.6 Atomic force microscopy for surface topography characterization

The important character of thin film is surface morphology and the favorite technique that uses for study surface morphology and roughness of nanoscale thin film is atomic force microscope (AFM). The AFM consists of a cantilever with a sharp tip (probe) at its end that is used to scan the specimen surface.

The cantilever is typically silicon or silicon nitride with a tip radius of curvature in the order of nanometers. When the tip is brought into proximity of a simple surface, forces between the tip and the sample lead to a deflection of the cantilever according to Hooke's law. Depending on the situation, forces that are measured in AFM include mechanical contact forces, van der Waals forces, etc.

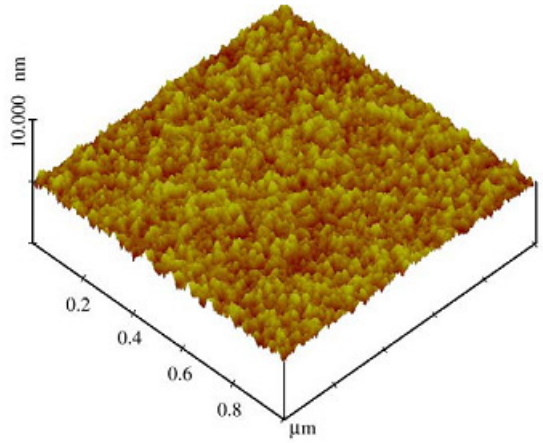

Figure 2.24 Example of AFM 3-D images surface roughness of Ti-doped DLC

The AFM can be operated in a number of modes, depending on the application. In general, possible imaging modes are divided into static (also called contact) modes and a variety of dynamic (or non-contact) modes where the cantilever is vibrated.

2.7 Effect of thermal heating to microstructure and material composition

The chemical bonding and elemental composition of DLC film normally were investigated by X-ray photoelectroscopy (XPS) and microstructiure of the film was also analyzed by Raman spectroscopy.

In 1984, R.O. Dillon et.al.[4] had investigated the disorder and crystallite formation of DLC film as a function of post-deposited annealing temperature. DLC film were deposited by ion-beam and rf-discharge deposition and annealed at temperature up to 950 ºC. I_D/I_G ratio shows maximum indicated that crystallite growth is promoted by higher anneal temperature. The shift of D and G lines to asymptotes of 1353 and 1598 cm^{-1}, respectively, as anneal temperature increases, indicates that crystallites are dominated by threefold (graphite) over fourfold (diamond) coordination. The line widths (full width of half maximum, FWHM) of both lines are also decreased with increasing annealing temperature. This is also consistent with the removal of bond-angle disorder and the increasing dominance of crystallites as annealing proceeds to higher temperature.

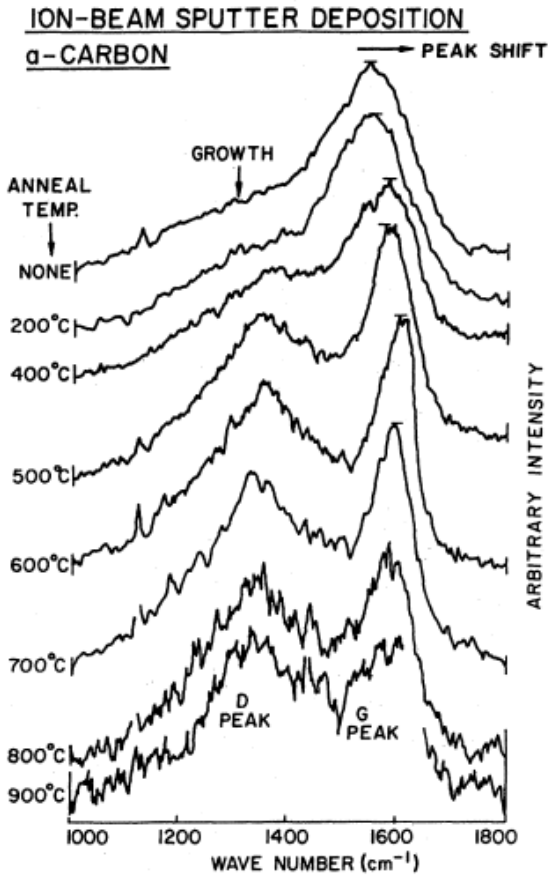

Figure 2.25 Raman spectra for a series of anneal temperature up to 900 ºC in an ion-beam-sputter-deposited sample

In 2006, H. Li et al. [7] studied the annealing effect of 520 nm thick hydrogenated DLC which deposited by plasma enhanced chemical vapor deposition. The Raman result shows no obvious change as compare to as-deposited film after annealing temperature below 200 ºC. but when the temperature above 200 ºC, the annealing cause effusion of

hydrogen and the sp^3 to sp^2 transformation led to the more graphite-like structure with poorer mechanical and tribological properties (friction coefficient and wear). G peak and D peak positions shift upwards and D peak intensity increases, which indicates a severe degradation of the structural properties i.e. the decreases of the sp^3 content and the diamond-like characterization and the increase of graphite-like component. The tribological properties also depend on the testing environment. C-O, C=O and O-C=O were observed at worn surface by XPS.

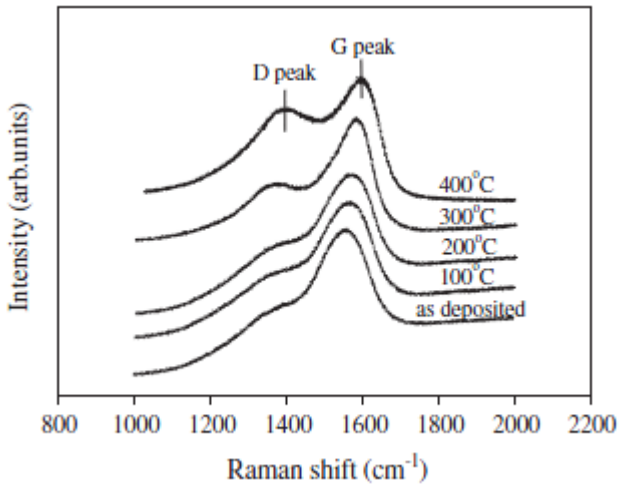

Figure 2.26 Raman spectra of as-deposited hydrogenated DLC films and annealed films at different temperatures

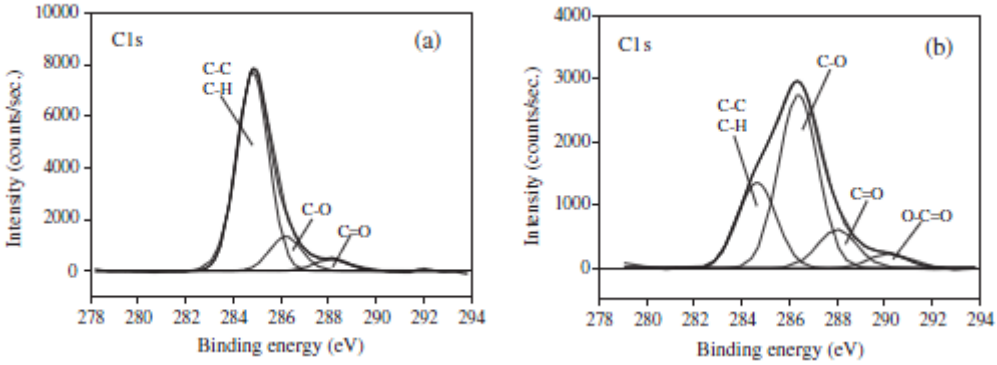

Figure 2.27 XPS spectra of C1s; (a) on the original surface of as-deposited hydrogenated DLC; (b) on the worn surface after friction testing in air (RH = 40%)

Two years later, S. Baek et al. [26] studied heating effect on 1.5 um thick DLC with similar deposition technique, RF-plasma-assisted chemical vapor deposition but this study is focusing on aging of heating. Raman shows that the increasing of aging time, the D peak and G peak move to higher wavenumber. The intensity ratio I_D/I_G increases which reflect strong graphitization of the DLC film due to breakup of the sp^3 structure at high temperature.

There are few of researchers studied the annealing effect on metal-doped DLC that will use as references in this section. M.C. Chiu et al. [6] used cathodic arc evaporation deposit Cr-doped DLC and then anneal in ambient air for 0.5 hr. the Raman spectra reveals the shift of G and D peak to higher wavenumber and observe the separation of D

and G peak at 300 ºC which the conversion of sp^3-bond carbon to sp^2-bond carbon occurred. Increase of I_D/I_G value conforming to the graphitization process of Cr-doped DLC films. Cr-doped DLC films annealed at temperature higher than 300 ºC, the carbon structure is converted to nonocystalling graphite and carbide. The evolution to nanocrystalline graphite must have been accompanied by conversion of sp^3 bonds to sp^2 bond.

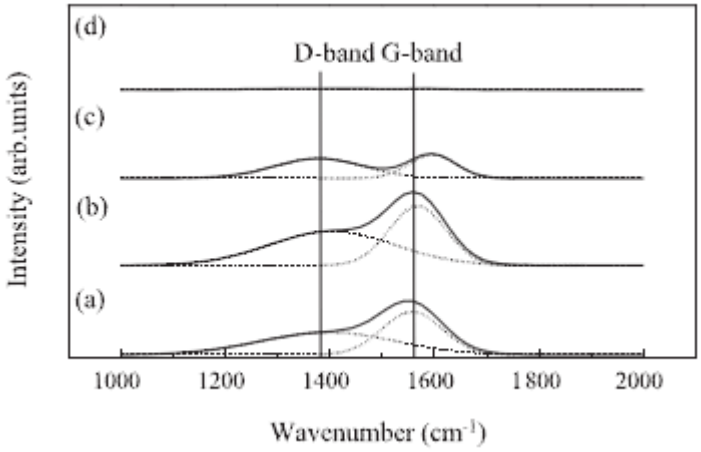

Figure 2.28 The dependence of Raman shift on the annealing temperature of (a) as-deposited, (b) annealed at 200 ºC, (c) annealed at 300 ºC, (d) annealed at 400 ºC DLC films.

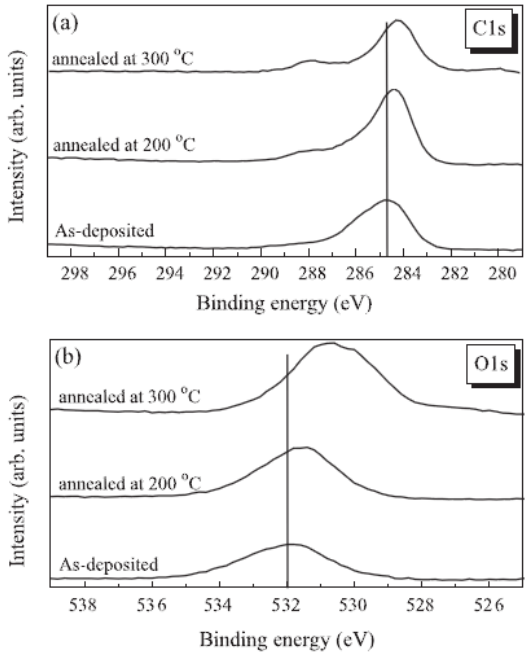

Figure 2.29 XPS spectra of the (a) C1s, and (b) O1s core level for annealed Cr-DLC films.

The spectral line shape of DLC C1s core level shift of specimen annealed at 300 ºC (Figure 2.29), the shift of binding energy to lower values have significantly been affected by oxidation which suggests the conversion of sp^3 site to sp^2 site of DLC films. After 300 ºC, the increase of relative intensity near 288.6 eV indicates formation of C-O

and C=O components which confirmed from the shift O1s spectra. For Cr-doped DLC, oxidation of Cr is more marked and more pronounced at higher temperature. At temperature lower than 200 ºC, oxygen is adsorbed on the surface and a significant oxidation occurs. Oxidation of carbon increases dramatically forming carbon dioxide, which effuse out of the surface, and with remaining carbon is mainly a graphite phase.

Results of annealing effect on Ti-doped DLC studied by Y.H. Lin et al. [9] are similar to Cr-doped DLC but Ti-doped DLC can retain the film structure up to 500 ºC. Figure 2.30 show the Raman result of Ti-doped DLC as a function of annealing temperature.

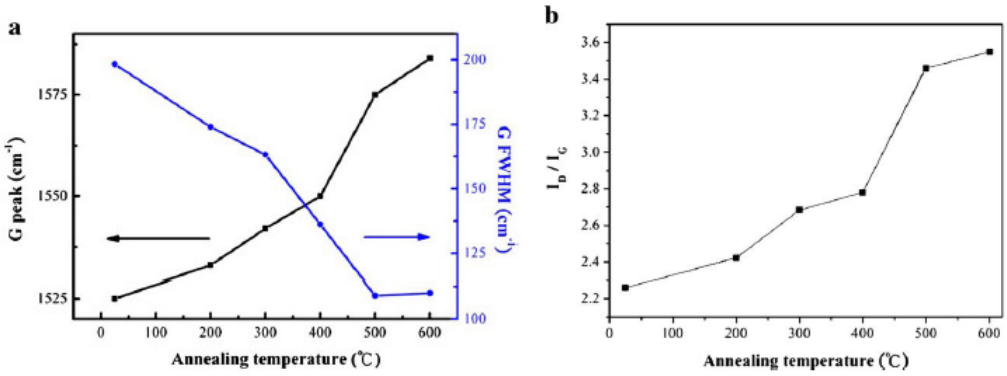

Figure 2.30 The annealing temperature evolved characters of the Ti-doped DLC films; (a) G-band position and full width at half maximum (FWHM); (b) I_D/I_G ratio.

The ta-C or ta-DLC which has highest %sp^3 was also deposited and then anneal for study the impact of temperature and time to structure and other properties. B.K. Tay et al. [27] study the annealing effect on 70 nm thick ta-C deposited by FCA. Films remain structurally stable after annealing in air at up to 300 ºC for 4 hr. Some degree of graphitization was observed on films annealed at 400 ºC, the films begin to oxidize and lose thickness only after annealing at 500 ºC for more than 2 hr. The narrowing and an upshifting of G peak together with an increase in the I_D/I_G ratio were observed during the first 2 hr of annealing, with the exception at 500 ºC in which the film deteriorates further as oxidation occurs. All Raman results are shown in Figure 2.31.

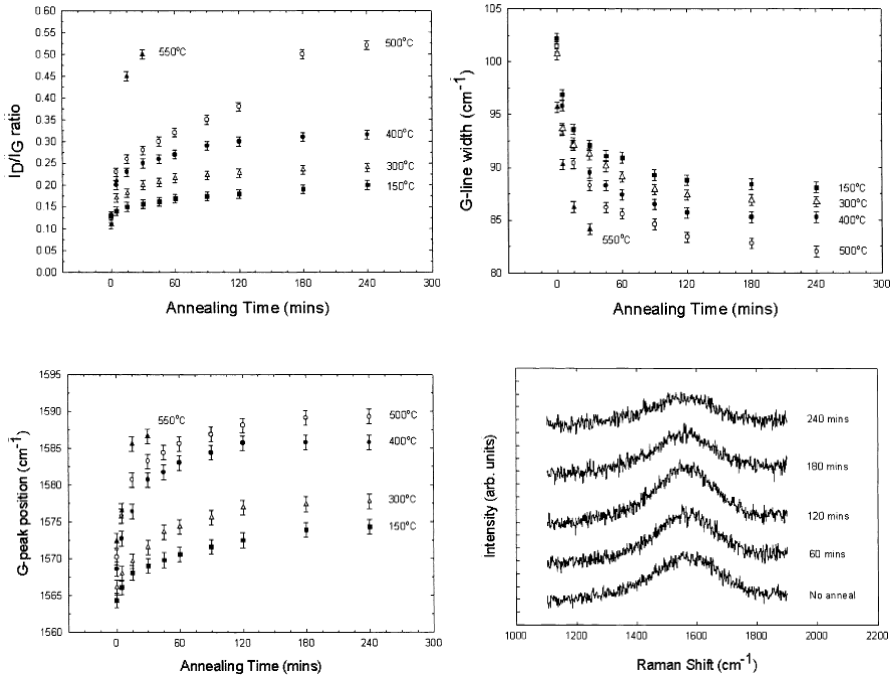

Figure 2.31 I_D/I_G ratio, G-line width, G peak position, peak intensity of ta-C as a function of annealing temperature.

R. Kalish et al. [28] studied the thermal stability and relaxation of 100 nm thick ta-C which deposited by mass selected ion beam deposition system with different sp^3 fraction. The ta-C skeleton stabilitzes the DLC so that clustering of graphitic domains, which starts at 427 ºC for the lower sp^3 films, does not occur event at 997 ºC for the films with 80% sp^3. Formation of sp^2 rings (without necessarily changing the sp^3 fraction) is another relaxation process which occurs for all DLC films. It is minor for a sp^3 rich ta-C, which seems to be relatively stable even at 997 ºC. The evolution of a distinct D peak indicates the formation of nm size graphitic domain. G peak position moves towards higher wavenumber which is not directly to the smaller sp^3 fraction , but rather to the larger sp^2 cluster size with smaller nearest neighbor distance. I_D/I_G changes versus annealing temperature shows the thermally induced clustering of graphitic domains in DLC films. This work results clearly show that the thermal stability of DLC films decreases with increasing of sp^2 fraction. The size of the sp^2 clusters which formed by thermal relaxation of DLC films increases with the initial sp^2 fraction, even in the absence of a sp^3 to sp^2 conversion, thus enabling the clustering of graphitic nanocrystallites.

Similar to J.O. Orwa et al. [29] who also studied the thermally induced sp^2 clustering in ta-C films prepared by FCA. G peak shifts to a higher frequency. In the vicinity of 600 ºC, the 1350 cm^{-1} D (disorder) peak, associated with the presence of nanometer-sized graphitic domains, appears and increases in intensity with subsequent annealing. Up to 300 ºC, G peak position different form each sample. An upward shift in the G peak position signifies the sp^2 carbon aggregation into larger clusters with smaller nearest neighbor distances. The D peak, which appears at higher annealing temperatures, indicates organization of sp^2 sites into nanoclustures of sp^2 rings. The nanoclusters can be formed either directly by clustering of the sp^2 component of the film or by sp^3 to sp^2 transformations followed by sp^2 clustering. I_D/I_G starts increase between 600-700 ºC, indicating than macroscopic clustering of sp^2 carbon begins in this temperature range.

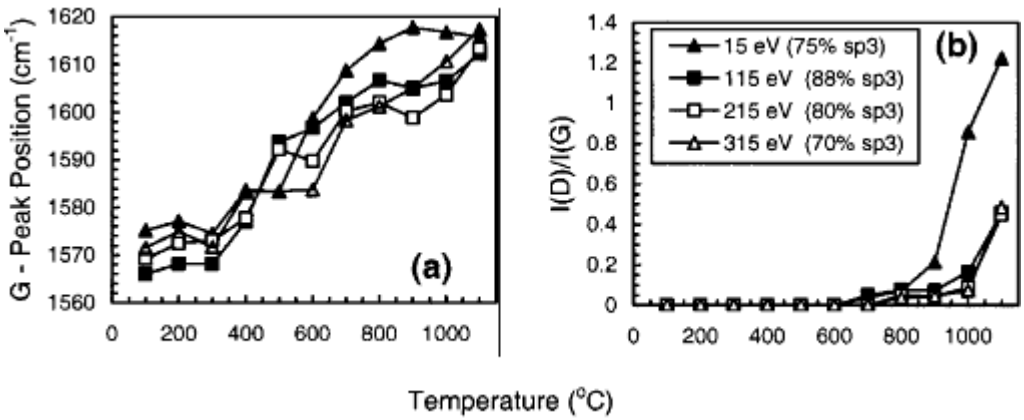

Figure 2.32 (a) G-peak position; (b) I_D/I_G vs. annealing temperature for all the samples studied. The legend, shown as an insert in Figure 2.29 (b), applies to Figure 2.29 (a).

Lately, Kamiya et al. [10] who compared various DLC films at few hundred nm thick with Raman observed that ta-DLC can be structurally stable at up to 700 ºC in N_2 atmosphere. The result obtained in their report showed that D and G peak of ta-DLC was split from each other after annealing at 750 ºC and performed as a great barrier coating after heating up to 800 ºC. In additional, the ta-DLC was also stable up to 500 ºC in air atmosphere without any change in Raman spectra.

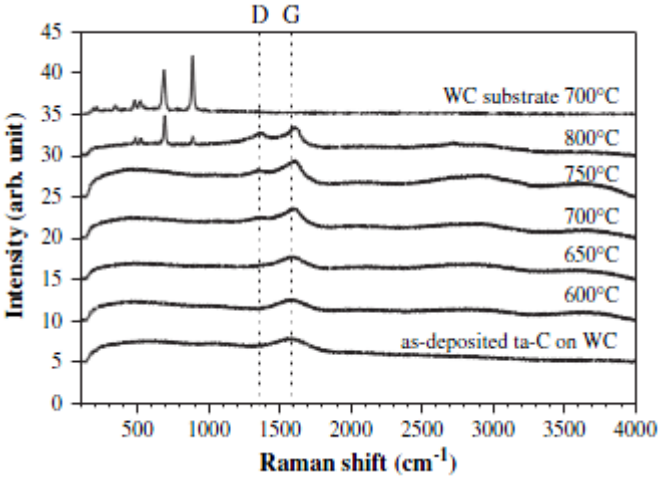

Figure 2.33 Raman spectra of ta-DLC(H) as a function of annealing temperature in N_2 for 1 hr

2.8 Effect of thermal heating to wear resistance of DLC

2.8.1 Wear behavior [30]

There has been extensive research in the past two decades in characterizing the tribological behavior of DLC films due to their high wear resistance and very low friction coefficients. The wear and friction of DLC films are greatly affected by:

(1) Nature of the film (controlled by deposition process)
(2) Tribotesting conditions
    (a) Material parameters (nature of the substrate)
    (b) Mechanical parameters (contact pressure, type of contact)
    (c) Kinematic parameters (nature of motion, speed)
    (d) Physical parameters (temperature during friction) and
    (e) Chemical parameters (nature of the environment such as relative humidity)

Thus, a wide range of tribological properties have been reported in the literature for DLC films. The tribological experiments conducted earlier have shown that DLC films are sensitive to the environmental parameters.

It is believed that the friction of DLC films is controlled by the formation of transfer layers during wear on the sliding couple, which generally has a lubricating effect. The very low friction and reasonably long life of DLC films is explained by a transfer buildup followed by an interfilm sliding mechanism in a velocity accommodation mode. Transfer layer formation is associated with significant wear in the initial stages. The interfilm sliding mechanism exists when a transfer layer forms at the contact area, not allowing physical contact between the DLC film and the counter surface of the pin. This transformation may be caused by friction induced annealing by thermal and strain effects generated during sliding. A wear-induced graphitization mechanism has been put forward by Liu and Meletis to account for the transfer layer formation and subsequent tribological behavior.

2.8.2 Effect of thermal heating on film wear resistance

In 2004, W. Zhang et al. [31] studied the effect of annealing on mechanical and tribological properties of DLC multilayer films. The films consisting of alternating sublayers of soft and hard DLC using plasma PVD deposition then films pass to anneal in vacuum at 250 ºC for 2 hr. As compare to single layer DLC which deposited as a control sample using same deposition technique, the anneal can help reduce internal stress on multilayer DLC and increase critical load but there is by-effect of this annealing which is film hardness and wear resistance decreasing.

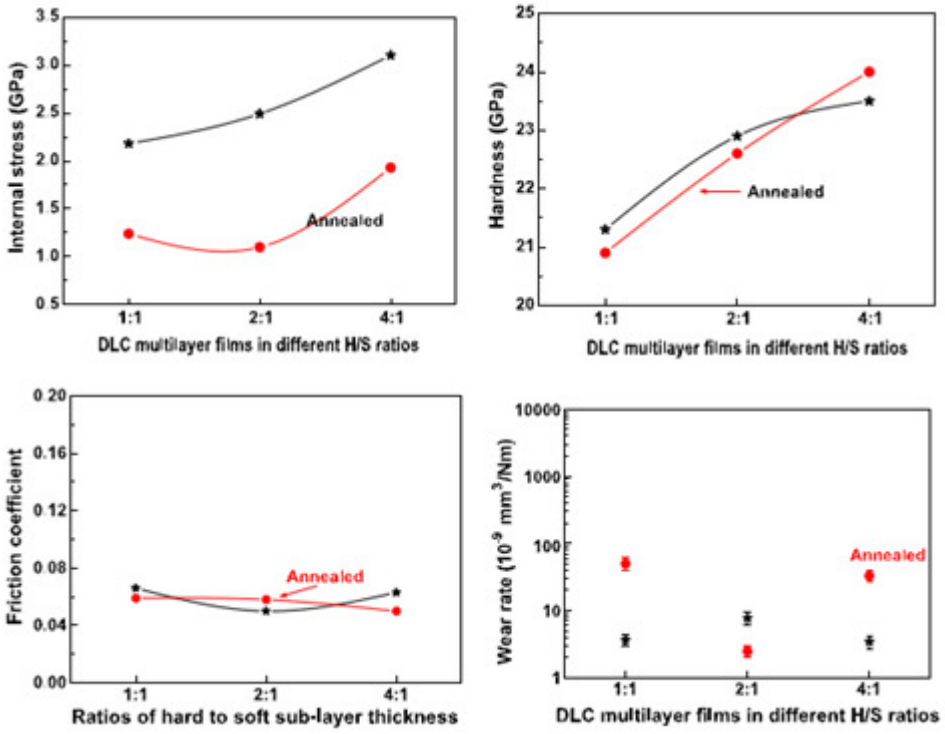

Figure 2.34 Internal stress, hardness, friction coefficient and wear rate of the DLC multilayer films before and after anneal.

In 2007, Edwin H.T. Teo et al. [32] also studied thermal stability of nonhydrogenated amorphous carbon prepared by FCA. The annealing after deposition process can help to reduce internal stress but decrease hardness and wear resistance same as result from W. Zhang et al. The wear rates for the multilayer films. All the films showed a general increase in wear rates after annealing. This was not surprising considering that the soft sublayers become more graphitic increase in sp^2 upon annealing and thereby lowering the wear resistance of the film.

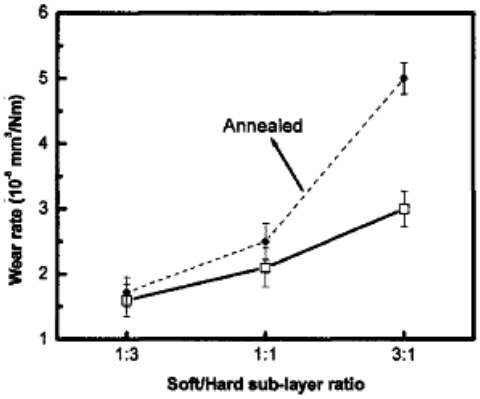

Figure 2.35 Wear rates before and after annealing for multilayer films of different soft to hard sublayer ratios.

2.9 Effect of thermal heating of surface roughness of DLC

On the study of annealing effect on the titanium-doped DLC films, the surface roughness as-depostied and after annealing was also considered. The film surface retains a smooth surface after annealing as shown in small variation Rms as a function of annealing temperature.

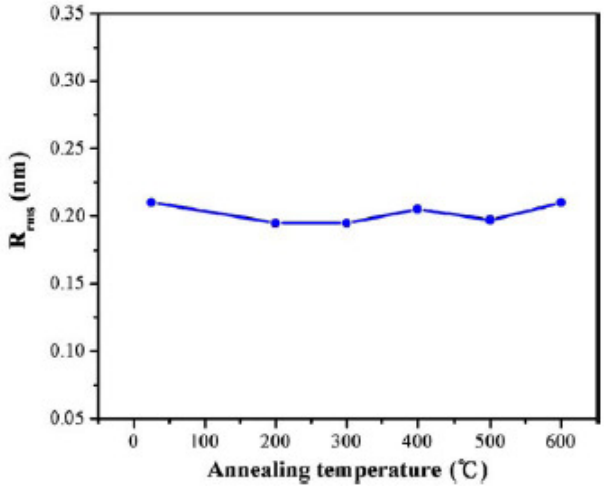

Figure 2.36 Slight variation of the measured Rrms around 0.2 for the Ti-doped DLC films annealed at various temperatures.

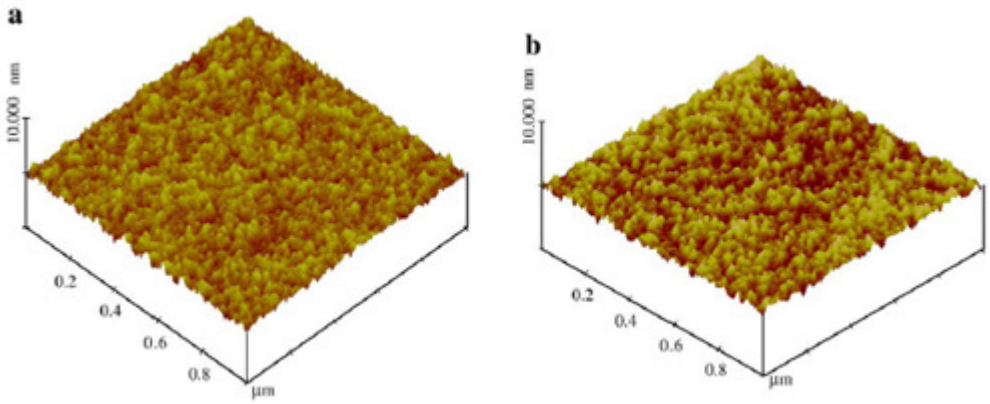

Figure 2.37 AFM 3-D images of Ti-doped DLC films (a) before annealing and (b) annealed at 600 °C.

J.O. Orwa et al. [29] also showed evolution of topographic of the ta-C films after annealing with different temperature. At 600 °C, the surface morphology changes; holes about 100 nm in diameter appear at the surface. Further annealing results in a dramatic increase in the surface roughness. Granular structures appear in the topographic images and become well defined with an increasing temperature. Figure 2.35 is Evolution of topographic and current image of ta-C film at different annealing temperature.

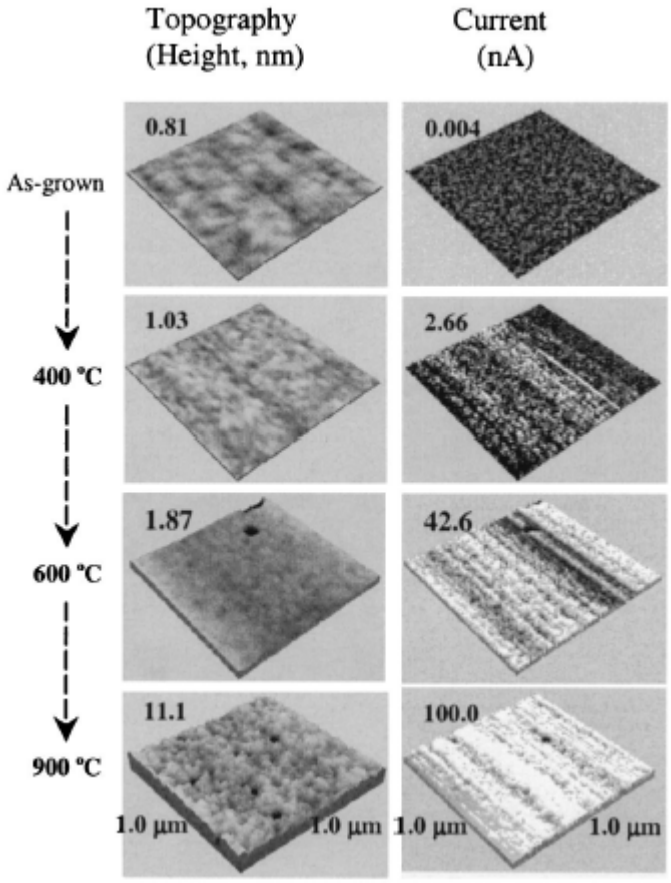

Figure 2.38 Evolution of topographic and current images (1x1 mm^2) of ta-C film (carbon ion energy 15 eV) with the increase of annealing temperature.